AD-A047 512 NAVAL WEAPONS CENTER CHINA LAKE CALIF F/G 9/5
CHARACTERISTICS OF LARGE MILLIMETER AND SUBMILLIMETER WAVE REFL--ETC(U)
OCT 77 W E KATZENSTEIN

UNCLASSIFIED NWC-TP-5980 NL

| OF |
AD
A047512

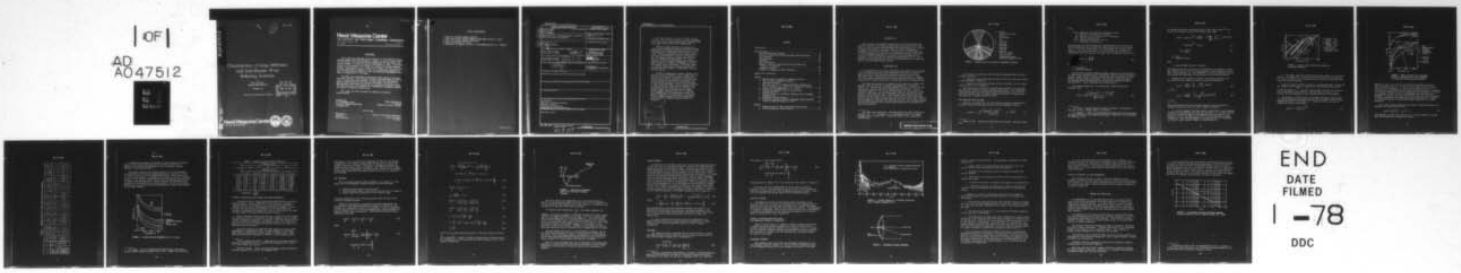

END
DATE
FILMED
1-78
DDC

NWC TP 5980

Characteristics of Large Millimeter and Submillimeter Wave Reflecting Antennas

by
West E. Katzenstein
Electronic Warfare Department

OCTOBER 1977

Naval Weapons Center
CHINA LAKE, CALIFORNIA 93555

Naval Weapons Center

AN ACTIVITY OF THE NAVAL MATERIAL COMMAND

W. L. Harris, Jr., RAdm., USN ..... Commander

R. M. Hillyer ..... Technical Director (Acting)

FOREWORD

This study was undertaken by the direction of the Naval Electronics Systems Command under Task X0738100 in support of the U.S. Navy preparatory effort for the 1979 General World Administrative World Radio Conference (GWARC) to be held in Geneva, Switzerland, in 1979. A shortened version of this document has evolved as a result of the Naval Weapons Center's participation in U.S. Study Group 1 (USSG 1) of the International Radio Consultative Committee (CCIR), an international organization that provides technical support to the International Telecommunications Union in preparation for the GWARC.

The CCIR is now examining interference between users of the spectrum above 100 GHz. This document discusses some advantages and limitations of large reflecting antennas at high frequencies and examines general characteristics of far and back sidelobes. The intent is to make possible provisional estimations of interference received through off-axis directions at millimeter and submillimeter wavelengths despite the absence of measured antenna data.

This report has been reviewed for technical accuracy by Donald Paolino.

Released by
G. R. SCHIEFER, *Head*
Electronic Warfare Department
4 October 1977

Under authority of
R. M. HILLYER
Technical Director (Acting)

NWC TP 5980

Published by . . . . . Technical Information Department
Collation . . . . . Cover, 11 leaves
First printing . . . . . 60 copies

INITIAL DISTRIBUTION

2 Naval Air Systems Command (AIR-954)
1 Naval Electronics Systems Command (ELEX-00BE, William J. Cook)
2 Naval Sea Systems Command (SEA-09G32)
12 Defense Documentation Center
1 Department of Commerce (Office of Telecommunications, R. J. Mayher)

UNCLASSIFIED

SECURITY CLASSIFICATION OF THIS PAGE *(When Data Entered)*

REPORT DOCUMENTATION PAGE

READ INSTRUCTIONS BEFORE COMPLETING FORM

(14) 1. REPORT NUMBER: NWC-TP-5980 ✓ | 2. GOVT ACCESSION NO. | 3. RECIPIENT'S CATALOG NUMBER

(6) 4. TITLE *(and Subtitle)*: CHARACTERISTICS OF LARGE MILLIMETER AND SUBMILLIMETER WAVE REFLECTING ANTENNAS.

(9) 5. TYPE OF REPORT & PERIOD COVERED: Final rept.,

6. PERFORMING ORG. REPORT NUMBER

(10) 7. AUTHOR(s): West, Katzenstein (E.)

8. CONTRACT OR GRANT NUMBER(s): 65535N

9. PERFORMING ORGANIZATION NAME AND ADDRESS: Naval Weapons Center, China Lake, CA 93555 (16) XØ738

10. PROGRAM ELEMENT, PROJECT, TASK AREA & WORK UNIT NUMBERS: NAVELEX (17) ~~Task~~ XØ738100

11. CONTROLLING OFFICE NAME AND ADDRESS: Naval Weapons Center, China Lake, CA 93555 (11) Oct 77

12. REPORT DATE: ~~October~~ Oct 1977

13. NUMBER OF PAGES: 20

14. MONITORING AGENCY NAME & ADDRESS *(if different from Controlling Office)* (12) 23p.

15. SECURITY CLASS. *(of this report)*: UNCLASSIFIED

15a. DECLASSIFICATION/DOWNGRADING SCHEDULE

16. DISTRIBUTION STATEMENT *(of this Report)*

Approved for public release; distribution unlimited

17. DISTRIBUTION STATEMENT *(of the abstract entered in Block 20, if different from Report)*

18. SUPPLEMENTARY NOTES

19. KEY WORDS *(Continue on reverse side if necessary and identify by block number)*

Interference
Millimeter reflecting antennas
Radiation patterns
Sidelobe antenna patterns
Submillimeter reflecting antennas

20. ABSTRACT *(Continue on reverse side if necessary and identify by block number)*

See back of form

DD FORM 1 JAN 73 1473 EDITION OF 1 NOV 65 IS OBSOLETE
S/N 0102-LF-014-6601

UNCLASSIFIED
SECURITY CLASSIFICATION OF THIS PAGE *(When Data Entered)*

403 019

4B

(U) *Characteristics of Large Millimeter and Submillimeter Wave Reflecting Antennas*, by West Katzenstein. China Lake, Calif., Naval Weapons Center, September 1977. 20 pp. (NWC TP 5980, publication UNCLASSIFIED.)

(U) This document examines characteristics of large reflecting antennas at short (millimeter and submillimeter) wavelengths, emphasizing analysis of their susceptibility to interference from off-axis directions. Allowable deviations from the desired reflecting surface are measured in terms of wavelengths; and, the required tolerances become severe at millimeter and submillimeter wavelengths. As a given reflector is used at higher frequencies, increasingly greater amounts of energy are scattered out of the main beam by surface deviations. This energy appears in a narrow-scatter pattern, however, and does not increase the susceptibility to interference from off-axis directions.

(U) Energy transmission at angles outside of main beam and the near sidelobes is due to energy from the feed not intercepted by the reflector (spillover), the diffraction pattern created by the reflector edge, energy scattered by the feed and its supports, and the interference patterns set up by the interaction of these three mechanisms. The far and back sidelobes of large reflecting antennas tend to diminish with increasing frequency, while the far sidelobe at the shadow boundary and the backlobe tend to remain constant. Thus, measured levels of far sidelobes, back sidelobes and the backlobe made at lower frequencies are useful for estimations of interference levels at higher frequencies, until measured data are available. An example reference pattern is presented.

CONTENTS

INTRODUCTION

This document will examine characteristics, achievable main beam radiation patterns, and frequency dependence of the far and back sidelobes of large reflector-type millimeter and submillimeter wave antennas. An antenna is generally considered large if it has a diameter-to-wavelength ratio greater than 100. A discussion of the susceptibility of these antennas to interference from other emitters and a curve indicating the maximum magnitudes of the near and far sidelobes will be presented. This curve must be regarded as provisional until it can be substantiated by measured data but is nevertheless useful for predicting levels of interference between systems.

CHARACTERISTICS

The requirements that a given millimeter wave antenna collect energy from a preferred direction, while suppressing terrestrial or galactic noise and signals from interfering emitters received from off-axis directions, place constraints on its entire radiation pattern. Thus, a full 2π-steradian radiation pattern must be characterized at millimeter frequencies to enable predictions of interference levels between systems.

The radiation pattern of an antenna can be broken into roughly four regions, which outline the mechanisms responsible for the pattern (Figure 1).[1] The mainlobe and near sidelobes, Region I, are the diffraction pattern caused by the feed illuminating the reflector. The far sidelobes, Region II, are the sum of feed energy not intercepted by the reflector (spillover) and the interference pattern created by the illumination of the reflector edge. The backlobes, Regions IIIA and IIIB, and the rearlobe, Region IV, are due to the reflector edge interference pattern alone since the reflector obscures the feed in this area. Specialized mathematical techniques have been developed for each of these regions; the resulting formulas can be used to make predictions concerning millimeter wave antennas.

---

[1] The Ohio State University. *The Wide Angle Side Lobes of Reflector Antennas*, by P. A. J. Ratnasiri, R. G. Kouyoumjian, and P. H. Pathak. Columbus, Ohio, 23 March 1970. (Technical Report 2183-1, publication UNCLASSIFIED.)

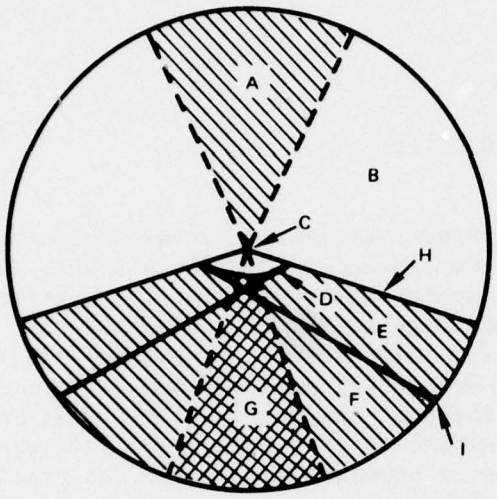

A: REGION I
FORWARD AXIAL REGION

B: REGION II
FAR SIDELOBES

C: FEED

D: REFLECTOR

E: REGION IIIA
BACKLOBES

F: REGION IIIB
BACKLOBES

G: REGION IV
REAR AXIAL REGION

H: SHADOW BOUNDARY

I: INTERFERENCE BOUNDARY
(TANGENT TO SURFACE AT EDGE).

FIGURE 1. Regions Used for Analysis of Radiation Pattern.

Two features of millimeter wave antennas distinguish them from lower frequency antennas:

1. Physically small reflecting surfaces can be very large with respect to the wavelength in question.

2. Physically realizable reflector surface tolerances can be a significant fraction of a wavelength.

The large amount of aperture available makes possible, in principle, the design of antennas with very sophisticated patterns. The relatively severe surface tolerance limitations create phase errors in the reflected radiation, however, and can scatter significant amounts of energy out of the intended or designed radiation pattern.

MAIN BEAM AND NEAR SIDELOBES

Equation 1 describes the far field radiation pattern created by illuminating a perfect reflecting surface with electromagnetic energy.[2]

$$G_p(\theta,\phi) = \frac{4\pi}{\lambda^2} \frac{\left| \int f(\bar{r}) e^{j\bar{k} \cdot \bar{r}} dS \right|^2}{\int [f(\bar{r})]^2 dS} \quad , \quad \bar{k} = \frac{2\pi}{\lambda} \overline{P_o} \qquad (1)$$

[2]Samuel Silver. *Microwave Antenna Theory and Design.* New York, Dover, 1965.

where

(θ,ϕ) = spherical coordinates of observation point
$\bar{r}$ = aperture vector position variable
$\overline{P_o}$ = unit vector in the direction of observation
dS = element aperture area
$f(\bar{r})$ = aperture illumination function
λ = wavelength of radiation

This expression involves mathematical approximations to the field coordinates which make it valid near the forward major axis of the antenna only. It does not include effects of feed blockage or tolerance limitations of the reflector surface. For the special case of uniform illumination over the aperture, the major axis (Z-axis) gain is given by

$$G_p(0,0) = \eta \left(\frac{\pi D}{\lambda}\right)^2 \tag{2}$$

η = efficiency
D = aperture diameter

Gravitational loading, thermal stresses, aging, and the limitations of fabrication processes result in deviations from the desired reflecting surface. These surface tolerance limitations cause deviations from the desired aperture phase distribution. The effects of perturbations of the aperture phase distribution function have been examined by Ruze[3] and Scheffler[4]. Their formalisms are presented here.

Ruze modified Equation 1 by introducing a phase perturbation function, $\delta(\bar{r})$.

$$G(\theta,\phi) = \frac{4\pi}{\lambda^2} \frac{\left| \int f(\bar{r}) e^{j[\bar{k} \cdot \bar{r} + \delta(\bar{r})]} dS \right|^2}{\int [f(\bar{r})]^2 dS} \tag{3}$$

---

[3]John Ruze. "Antenna Tolerance Theory--A Review," *Proceedings of IEE*, Vol. 54, No. 4 (April 1966), pp. 633-640.

[4]H. Scheffler. "Über die Genauigkeitsforderungen bei der Herstellung optischer Flächen für astronomische Teleskope," Zeitschrift für Astrophysik 55, 1962, pp. 1-20.

By assuming that phase perturbations have a mean square value $\overline{\delta^2}$ and a correlation distance C across the aperture, Ruze found

$$G(\theta,\phi) = G_p(\theta,\phi)e^{-\overline{\delta^2}} + \left(\frac{2\pi C}{\lambda}\right)^2 e^{-\overline{\delta^2}} \sum_{n=1}^{\infty} \frac{\overline{\delta^2}^{\,n}}{n \cdot n!} e^{-(\pi Cu/\lambda)^2/n}$$

$$= G_p(\theta,\phi)e^{-\overline{\delta^2}} + G_s(\theta) \tag{4}$$

$$\overline{\delta^2} = \left(\frac{4\pi\varepsilon}{\lambda}\right)^2 \tag{5}$$

where

u = sin θ
n = summation index

ε = effective RMS reflector tolerance.

The radiation pattern is the sum of the pattern in the absence of tolerance limitations, G_p, which has been degraded by the exponential factor, and a scatter pattern, G_s. The assumption of uniform illumination across the aperture has been made in the derivation of the scatter pattern.

Scheffler (see Footnote 4) derived a closed-form expression for the scatter pattern, which is valid for uniform illumination.

$$G_s(\theta) = \left(\frac{2\pi C}{\lambda}\right)^2 \left[1 - e^{-\overline{\delta^2}}\right] e^{-(\pi Cu/\lambda)^2} \tag{6}$$

for $\overline{\delta^2} \leq 1$

$$G_s(\theta) = \left(\frac{2\pi C}{\lambda}\right)^2 \frac{\left[1 - e^{-\overline{\delta^2}}\right]}{\overline{\delta^2}} e^{-(\pi Cu/\lambda)^2/\overline{\delta^2}} \tag{7}$$

for $\overline{\delta^2} \geq 1$

These equations describe the following important characteristics of reflector antennas as they are used at higher frequencies.

1. As the frequency increases the main axis gain of a given antenna increases to some maximum value and then decreases. The initial increase is due to the growing number of wavelengths across the aperture; the decrease is due to the exponential factor that predominates at higher frequencies. This limiting behavior in attainable gain is illustrated for several large antennas (Figure 2) (see Footnote 3).

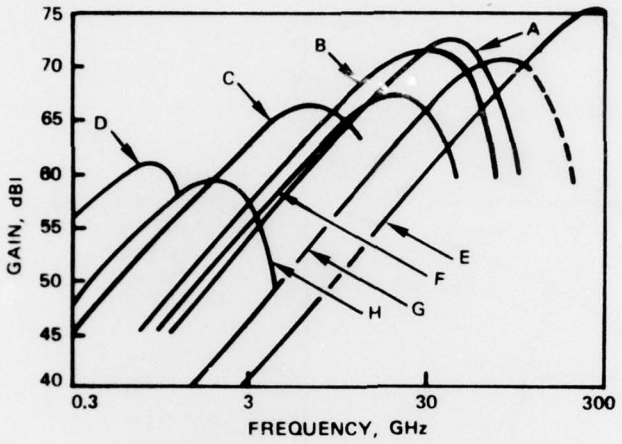

FIGURE 2. Gain of Large Paraboloids (Based on Published Estimates).

2. The energy lost from the principal pattern appears in the scatter pattern. The magnitude of the scatter pattern increases with frequency for a given reflector and illumination function until the magnitude dominates the principal pattern.

Thus, as a given reflector is used at increasingly higher frequencies, the energy received from or transmitted to a given target will suffer a loss described by $e^{-\overline{\delta^2}}$, and the received noise level will be increased due to the larger scatter pattern. The increase of noise will be a function of the environment in the pointing direction of the antenna.

The effects of surface errors on the main axis gain of the primary and scatter radiation patterns are plotted for a 10-meter reflector with assumed efficiency of 0.8 (Figure 3). Equations 2 and 4 are used to express the primary on-axis gain.

$$G_p(0,0) = \eta \left(\frac{\pi D}{\lambda}\right)^2 e^{-\overline{\delta^2}} \qquad (8)$$

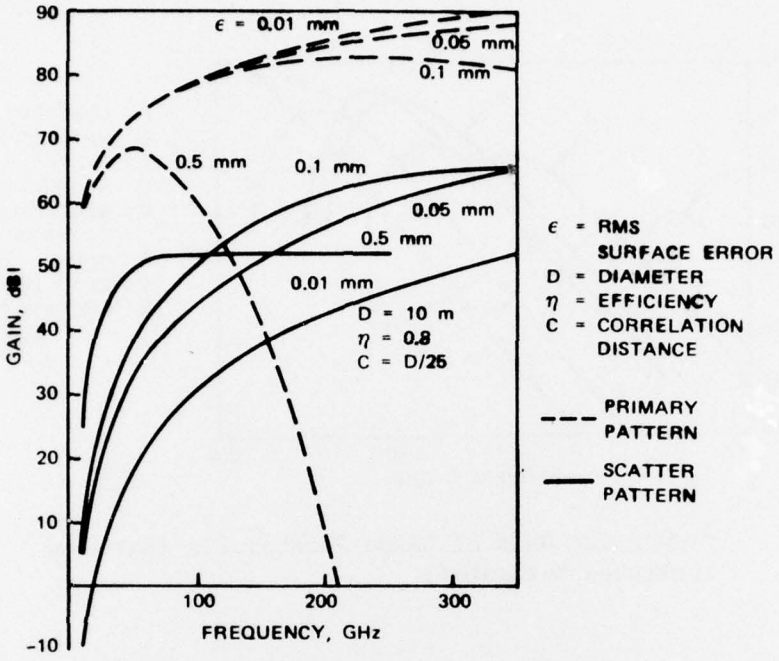

FIGURE 3. Main Axis Gain for a 10-meter Reflector (Primary and Scatter Patterns) as a Function of Mechanical Tolerance.

Equations 6 and 7 are used for the scatter pattern main axis gain. Table 1 indicates that $\varepsilon = 0.5$ mm is a worst case, 0.1 mm is typical, and 0.05 mm is attainable. $\varepsilon = 0.01$ mm is included in Figure 3 to illustrate the advantages available from improved fabrication techniques. A correlation distance of D/25 is assumed since Ruze measured a correlation distance of about D/25 for the HAYSTACK radio telescope (see Footnote 3). Figure 3 indicates that greater precision allows operation at higher frequencies and shows that the principal pattern is dwarfed by the scatter pattern at sufficiently high frequencies for a given precision.

The on-axis scatter pattern gain reaches a limiting value given by Equation 9 at large values of $\overline{\delta^2}$.

$$G_s(0) = \left(\frac{C}{2\varepsilon}\right)^2 \quad \text{for } \overline{\delta^2} >> 1 \tag{9}$$

This behavior is seen in the curve for $\varepsilon = 0.5$ mm in Figure 3, noting that $\overline{\delta^2}$ increases with frequency for fixed ε.

TABLE 1. Charateristics of Some Large Reflecting Antennas.

Property	Units	MIT Lincoln Lab.	Crimean RT-22 USSR	The Aerospace Corp. El Segundo, Calif.	The University of Texas, Austin			AFCRL Waltham, Mass.	Bonn Univ. (MPI) Germany	CRC (DRTE) Ottawa, Canada	NRAO Kitt Peak Mountain Tucson, Ariz.			Univ. of Calif. Berkley	JPL Pasadena, Calif.	FCRAO Amherst, Mass.		Chalmers Univ. Gothenburg, Sweden	Crawford Hill, N.J.
Diameter	meters	8.53	22.0	4.57	4.87			8.84	10.0	9.14	11.0			6.10	5.49	13.72		20.12	7.0
Optics		Cass.	Cass.	Cass.	Prime Focus			Cass.	Cass.	Cass.	Prime Focus			Cass.	Cass.	Cass.			
F/D		0.440		0.300	0.500			0.300	0.433	0.300	0.800			0.420	0.480				
Tolerance (mechanical)	mm		0.12	0.05	0.06			0.15	0.34		0.10			0.15	0.18	0.08		0.30	0.1
(Ruze method)	mm	0.20			0.10					0.53	0.15				0.18				
Frequency	GHz	35 | 90	75	94	35	97	134	35	36	35	31.4	85	260	38		115	300	150 max	300 max
Beamwidths	deg	.072 |	0.033	0.047	.110	.042	.033	0.067	0.055	0.070	.060	.020	.010			.011	.007		
Sidelobes	dB	24		22	23	22	22	18	20	16									
Date began operation		1961	1966	1963	1963			1965	1966	1966	1967			1968	1970	1976		1977	1977

A computerized analysis of the gain of large reflecting antennas using infinite series expressions for the scatter pattern as in Equation 4 has yielded on-axis behavior with increasing frequency similar to that presented here.[5]

The angular spread of the scatter pattern is of great importance for prediction of interference between equipments. Equations 6 and 7 are used to predict the 3- and 10-dB points of the scatter pattern for ϵ = 0.1 mm as a function of frequency for a family of reflector diameters (Figure 4). The scatter pattern narrows with increasing frequency until it reaches some limiting value. Table 2 presents the limiting values reached for a cross section of tolerance values. Note that the scatter patterns are very narrow, even for an extreme worst case 0.5-mm tolerance and a 1-meter diameter.

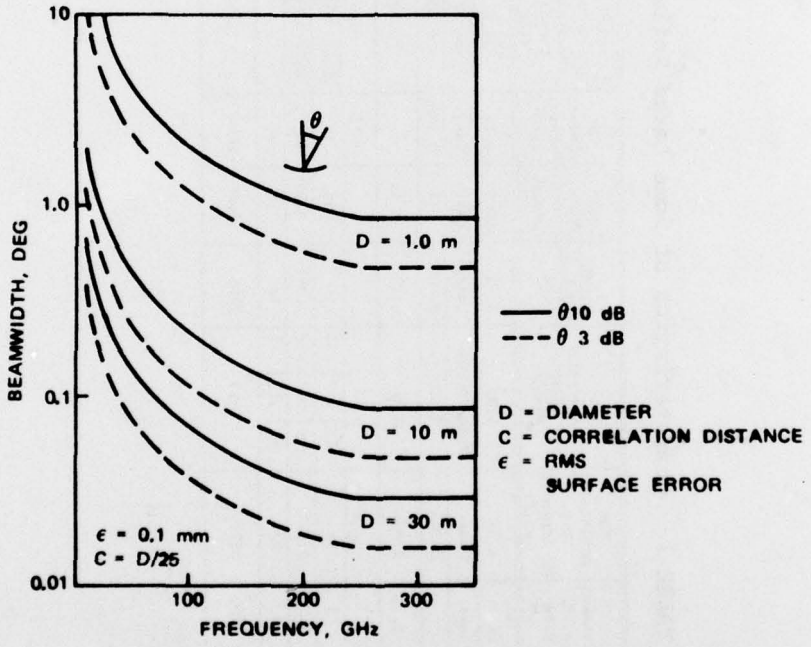

FIGURE 4. Scatter Pattern Beamwidth for ϵ = 0.1 mm.

[5] H. Zucker. "Gain of Antennas With Random Surface Deviations." The *Bell System Technical Journal*, Vol 47, No. 8 (1968), pp. 1637-1651.

TABLE 2. Limiting Scatter Pattern Beamwidth.

ε, mm	Diameter, meter					
	1.0		10		30	
	Beamwidth, deg[a]					
	$\theta_{3\ dB}$	$\theta_{10\ dB}$	$\theta_{3\ dB}$	$\theta_{10\ dB}$	$\theta_{3\ dB}$	$\theta_{10\ dB}$
0.01	0.048	0.087	0.0048	0.0087	0.0016	0.0029
0.03	0.143	0.261	0.014	0.026	0.0048	0.0087
0.05	0.239	0.435	0.024	0.043	0.0080	0.0145
0.10	0.477	0.869	0.048	0.087	0.0159	0.0290
0.20	0.954	1.74	0.095	0.174	0.0318	0.0580
0.30	1.43	2.61	0.143	0.261	0.0477	0.0869
0.40	1.91	3.48	0.191	0.348	0.0636	0.116
0.50	2.39	4.35	0.239	0.435	0.0795	0.145

[a] Beamwidth = $\frac{b}{\theta}$

SURVEY OF LARGE REFLECTING ANTENNA MAIN BEAM PERFORMANCE

The construction of large antennas with high precision is particularly difficult. Table 1 summarizes characteristics of a number of large millimeter wave antennas.[6] Note that attainable mechanical precision for structures approximately 10 meters in diameter is about 0.10 mm, and that tolerances as measured by the Ruze method (see Footnote 3) (examining the exponential decay in on-axis gain) are about one-half larger than mechanically measured tolerances.

Figure 2 presents the main axis gain for a number of large antennas. The exponential decay in performance at high frequencies due to surface errors as predicted by Equation 4 is evident. Note that large main beam gains at millimeter wavelengths (frequencies greater than 10 GHz) are generally more readily attained with smaller antennas since they can be made with greater precision.

The state-of-the-art in radio astronomy antennas for use at short wavelengths is represented by the 13.7-meter diameter Five Colleges Radio Astronomy Observatory (FCRAO) antenna at Amherst, Mass., which will provide precision operation to 300 GHz.[7] This antenna has main

[6] John R. Cogdell and others. "High Resolution Millimeter Reflector Antennas," *IEEE Transactions on Antennas and Propagation*, Vol. AP-18, No. 4 (July 1970), pp. 515-529.

[7] Michael O'Bryant. "Radio Astronomy Millimeter Antenna Dedicated," *Microwave Journal*, Vol. 19, No. 11, November 1976.

axis gain of 79, 81, and 80 dB at frequencies of 100, 200, and 300 GHz, respectively. The roll-off in gain above 200 GHz results from an RMS surface tolerance of 0.08 mm. The antenna is designed for minimal deformation due to gravity and is covered by a 20.7-meter-diameter radome with a controlled environment to minimize weather effects on the parabola. Several other large radio astronomy antennas can be used at frequencies up to 300 GHz.

FAR SIDELOBES

The far sidelobe radiation pattern (Region II in Figure 1) is the power sum of electromagnetic energy radiated by three mechanisms.

1. Energy radiated directly from the feed.
2. Reflected energy which is scattered by the feed and its supports.
3. Energy radiated by diffraction at the reflector edge.

Tolerance limitations of the reflecting surface have no direct effect on the far sidelobe patterns.

Ratnasiri, Kouyoumjian, and Pathak have derived expressions for the diffracted field using the geometrical theory of diffraction (see Footnote 1). Using their results, it is possible to write an expression for the radiation pattern in the far sidelobe area, valid everywhere in Region II except near its boundaries. This expression ignores energy scattered by the feed.

$$G_{E,H}(\theta) \propto T1_{E,H}(\theta) + T2_{E,H}(\theta) + T3_{E,H}(\theta) \tag{10}$$

where

$$T1_{E,H}(\theta) = \frac{f_{E,H}^2(\alpha)}{Ro^2(8\pi k)} \frac{D}{\sin\theta}\left[B_{E,H}^2(\theta) + C_{E,H}^2(\theta) + 2B_{E,H}(\theta)C_{E,H}\sin(kD\sin\theta)\right] \tag{11}$$

$$T2_{\substack{E\\H}}(\theta) = \frac{S_E \; f_E(\alpha) \; f_E(\pi - \theta)}{Ro\sqrt{\pi k}} \sqrt{\frac{D}{\sin\theta}} \left[B_{\substack{E\\H}}(\theta) \right.$$

$$\cos\left(kRo + \frac{\pi}{4} - \frac{kD}{2}\sin\theta + kF\cos\theta\right)$$

$$\left. + C_{\substack{E\\H}}(\theta) \cos\left(kRo - \frac{\pi}{4} + \frac{kD}{2}\sin\theta + kF\cos\theta\right)\right] \tag{12}$$

$$T3_{\substack{E\\H}}(\theta) = \frac{1}{2} f^2_{\substack{E\\H}}(\pi - \theta) \tag{13}$$

$$S_E = \frac{\cos\theta}{|\cos\theta|} \qquad S_H = -1 \tag{14}$$

$$B_{\substack{E\\H}}(\theta) = \frac{1}{\cos\left(\gamma + \frac{\theta}{2}\right)} \pm \frac{1}{\cos\left(\beta + \frac{\theta}{2}\right)} \tag{15}$$

$$C_{\substack{E\\H}}(\theta) = \frac{1}{\cos\left(\gamma - \frac{\theta}{2}\right)} \pm \frac{1}{\cos\left(\beta - \frac{\theta}{2}\right)} \tag{16}$$

$$\gamma = \frac{\pi}{4} - \frac{1}{2}\tan^{-1}\left(\frac{2F}{D} - \frac{D}{8F}\right) \tag{17}$$

$$\beta = \frac{3\pi}{4} - \tan^{-1}(4F/D) + \frac{1}{2}\tan^{-1}\left(\frac{2F}{D} - \frac{D}{8F}\right) \tag{18}$$

$$k = \frac{2\pi}{\lambda} \tag{19}$$

$f_{\substack{E\\H}}(\theta)$ is the E plane radiation pattern of the feed, measured relative to its major axis. Figure 5 defines the geometrical variables used in this expression. G_E and G_H describe the power radiated in the E and H planes, respectively.

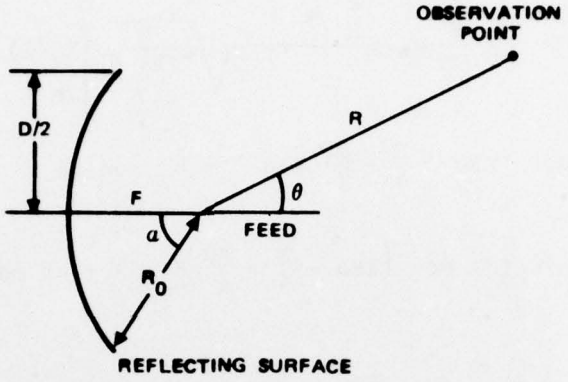

FIGURE 5. Geometrical Parameters Used in Far and Back Sidelobe Analysis.

The first term of this expression, T1, is the power radiation pattern of the diffracted energy, the third term, T3, is the pattern of the unintercepted feed energy, and the second term, T2, is caused by the interaction of the feed and diffraction energy.

If constant feed illumination, $f_{E_H}(\theta)$, and antenna geometry are assumed, then certain statements concerning the effects of using a given reflector at higher frequencies can be made. The only frequency dependence in this expression is in the wave number, k. Since the quantity kF will be much larger than π at millimeter wavelengths, the occurrence of k in the cosine and sine terms in T1 and T2 will result in their rapid oscillation between ±1 with small changes in θ resulting in a fine structure to the overall pattern. Changes in k will shift the phase of this fine structure, but not seriously alter the magnitudes of it peaks.

The wave number enters also as a multiplicative constant, $1/k$, in the first term of Equation 10, and as a multiplicative constant $\sqrt{1/k}$ in the second. With increasing frequency (increasing k) the contributions of the first and second terms will decrease while the third term will remain constant if a fixed illumination function is assumed.

Thus, it can be concluded that the far sidelobes of an antenna will diminish as a given reflector with fixed illumination is used at higher frequencies if scattering of reflected energy by feed structures is ignored.

SHADOW BOUNDARY

An important far sidelobe occurs near the boundary separating Regions II and IIIA due to the in-phase addition of direct feed radiation with energy diffracted by the reflector edge. Ratnasiri and others, have derived expressions for the radiated fields at the boundary (see Footnote 1). These expressions involve Fresnel integrals and are sufficiently complicated to require computerized analysis for precise computations. In another publication, however, Kouyoumjian and Pathak present a series expansion for the Fresnel integrals, and an analysis of the wave number (k) dependence of the power transmitted at the shadow boundary is possible, using only the lowest order term of the expansion.[8] The resulting gain function has a term proportional to D, a term highly oscillatory which is roughly proportional to $\sqrt{D/k}$, and a highly oscillatory term roughly proportional to 1/k. For a 1-meter reflector and a frequency of 100 GHz, the second and third terms are 17 and 33 dB below the first, respectively. The first term is therefore dominant at millimeter frequencies and is given by

$$G_{\substack{E\\H}}(\theta) \propto f^2_{\substack{E\\H}}(\theta) \left\{ \frac{D}{Ro}\left(\frac{1}{\sin\theta}\right) + 1 + S_{\substack{E\\H}} \sqrt{\frac{D}{Ro(2\sin\theta)}} \cos X \right\} \quad (20)$$

where

$$X = \left[2kRo \cos^2 \left(\gamma + \frac{\theta}{2}\right) - kRo + \frac{Dk}{2}\sin\theta - Fk\cos\theta \right] \quad (21)$$

This expression is valid near the shadow boundary, for which $\theta = 2\gamma$. Equation 20 indicates that the power near the shadow boundary is the sum of direct feed energy (second term), diffracted energy (first term), and a fine structure resulting from the interaction of these two (third term).

It can be concluded that the peak in the far sidelobes at the shadow boundary will tend to remain constant in magnitude as a given reflector with a fixed illumination function is used at higher frequencies.

BACKLOBES

The radiation pattern in Regions IIIA and IIIB of Figure 1 results from edge diffraction alone since the feed is blocked by the reflector. The radiated power in Region IIIA is described by

$$G_{\substack{E\\H}}(\theta) \propto \left(\frac{f_{\substack{E\\H}}(\alpha)}{Ro} \right)^2 \frac{D}{\sin\theta} \frac{1}{8\pi k} \left[B^2_{\substack{E\\H}}(\theta) \right] \quad (22)$$

[8] Robert G. Kouyoumjian and Prabhaker H. Pathak, "A Uniform Geometrical Theory of Diffraction for and Edge in a Perfectly Conducting Surface," *Proceedings of the IEEE*, Vol. 62, No. 11 (November 1974), pp. 1448-1461.

The pattern in IIIB is described by

$$G_{\substack{E \\ H}}(\theta) \propto \left(\frac{f_{\substack{E \\ H}}(\alpha)}{Ro} \right)^2 \frac{D}{\sin\theta} \frac{1}{8\pi k} \left[B^2_{\substack{E \\ H}}(\theta) + C^2_{\substack{E \\ H}}(\theta) + B_{\substack{E \\ H}}(\theta) C_{\substack{E \\ H}}(\theta) \sin(kD \sin\theta) \right] \quad (23)$$

The expression for Region IIIA is not valid near the boundary of Region II.

Note that the overall magnitudes of the patterns described by Equations 22 and 23 are diminished by the factor 1/k as the frequency of operation increases with all other parameters being held constant. Thus, the rear sidelobes will become smaller with increasing frequency.

REAR AXIS PATTERN

The geometrical theory of diffraction cannot be applied on the rear axis since it is a caustic for the diffracted rays (see Footnote 1). Ratnasiri and others have derived an expression for the pattern maximum which occurs on the rear axis using the ring current method. This expression is frequency independent. Thus, a given reflector will tend to demonstrate no change in the magnitude of the rear pattern maximum as it is used at higher frequencies with fixed illumination.

EXAMPLE OF PATTERN PREDICTION USING THE GEOMETRICAL THEORY OF DIFFRACTION

Figure 6 (from Footnote 1) compares a measured antenna pattern with a pattern calculated using the geometrical theory of diffraction for a prime focus-fed parabolic reflector with a diameter of 20.3λ at 10 GHz. Note the excellent agreement between the measured and predicted patterns. The occurrence of a peak in the far sidelobes near the shadow boundary is shown in this figure.

CASSEGRAIN ANTENNAS

Many antennas used at microwave and millimeter frequencies are of the Cassegrain geometry (Figure 7). The far and back sidelobe patterns of the Cassegrain antenna will differ somewhat from those of the prime

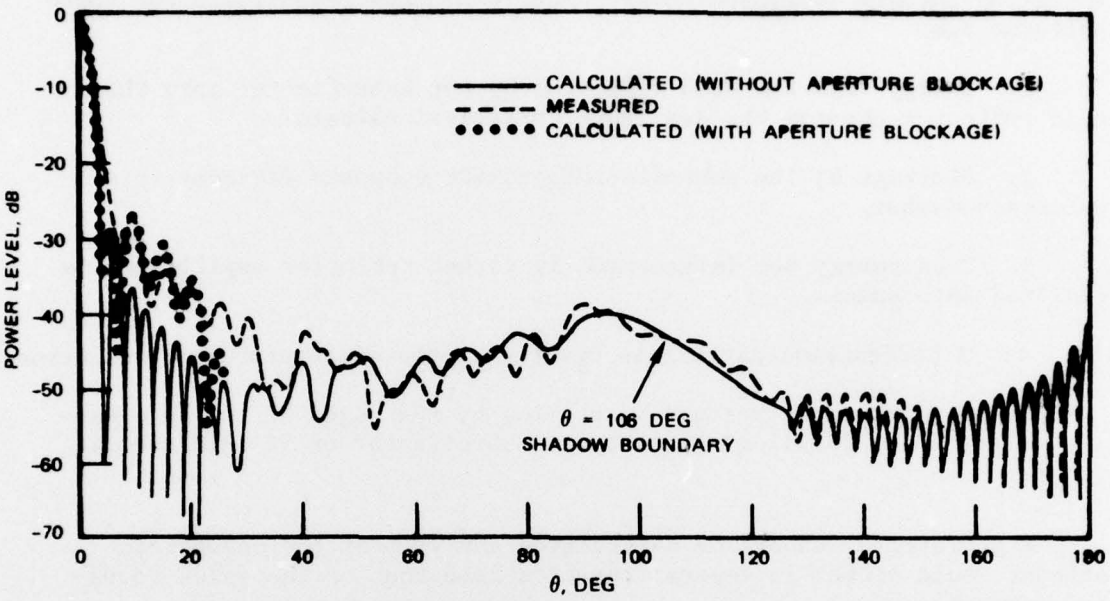

FIGURE 6. E-Plane Pattern of a Parabolic Reflector with a Flanged Waveguide Feed.

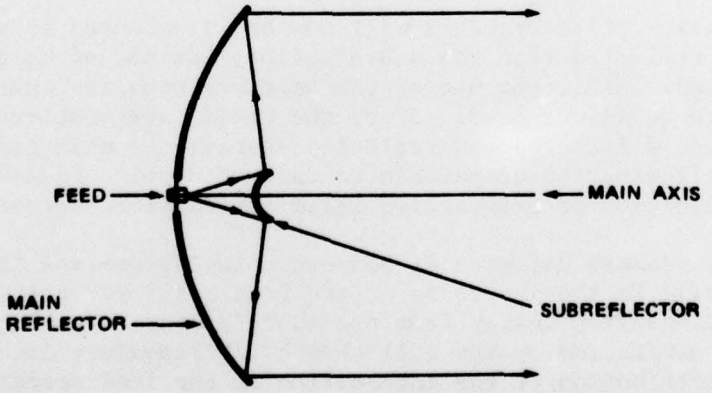

FIGURE 7. Cassegrain Antenna Geometry.

focus-fed antenna discussed above. The mechanisms responsible for these patterns are:

1. Energy from the feed reflected by the subreflector onto the main reflector creates the desired or principal pattern.

2. Blockage by the subreflector and its supports degrades this pattern somewhat.

3. Feed energy not intercepted by either reflector (spillover) is radiated into space.

4. A diffraction pattern is created by the edges of the subreflector.

5. A diffraction pattern is created by the edges of the main subreflector, which is illuminated by the subreflector or its diffraction pattern.

A geometrical theory of diffraction analysis of the Cassegrain antenna would differ in several respects from that of the prime focus-fed antenna:

1. The spillover radiation from the feed becomes inverted with angle since the feed is pointed along the main reflector axis instead of against it. Thus, the main feed sidelobes will be closer to the antenna main forward axis.

2. The diffraction energy due to the subreflector being illuminated by the feed will be introduced.

3. The main reflector edges will now be illuminated by energy either diffracted or reflected from the subreflector, instead of by energy directly from the feed. Efficient use of the aperture requires that most or all of the aperture be illuminated. Since the fields are continuous at the boundary between diffracted and reflected energy, the main reflector edge will receive illumination comparable to that of a prime focus-fed antenna, for either reflection or diffraction illumination (see Footnote 8).

Thus, the primary differences between prime focus- and Cassegrain-fed antennas will be the inversion of the feed spillover pattern and the addition of diffraction energy from the subreflector. The angular distribution of the diffracted energy will show a $1/k$ frequency dependence, and the angular distribution of the interaction of the feed energy with the diffraction energy will show a $\sqrt{1/k}$ dependence, as in terms one and two of Equation 10, respectively.

It can be concluded that the far sidelobes, rear sidelobes, and backlobe will show the same general improvement with increasing frequency for fixed illumination function for a Cassegrain-fed antenna as for a prime focus-fed antenna. The principal pattern degradation with increasing frequency, due to surface tolerance limitations, will be the same for either feed type.

VALIDITY OF ANALYSIS AT HIGH FREQUENCIES

The tolerance analysis is valid to optical frequencies, since Scheffler's analysis of the scattered pattern was done for optical devices (see Footnote 4). The diffraction analysis does not include irregularities in the diffracting edge or edge thickness which may become more important at higher frequencies.

SUMMARY AND CONCLUSIONS

The degradation of the principal pattern due to tolerance limitations of the reflecting surface is the main obstacle to utilization of large reflectors above 100 GHz. As a given reflector is used at higher frequencies, assuming fixed illumination, its gain reaches a limiting value and then diminishes. This lost energy appears in a narrow scatter pattern, which becomes larger than the principal pattern at sufficiently high frequency.

The appearance of the scatter pattern due to tolerance limitations of the reflecting surface will result in increased probability of receiving undesired emissions from threat emitters. This pattern is narrow, however, as shown in Table 2, and good system design can preclude interception of unwanted emissions.

Far sidelobe levels will generally decrease as parabolic reflectors are used at higher frequencies. Tolerance limitations in the reflecting surface do not impact on far or backlobe levels. Thus, immunity to energy received through the far sidelobes will increase.

The sidelobe near the shadow boundary caused by in-phase addition of feed spillover and diffracted energy will tend to remain constant at higher millimeter wave frequencies.

Backlobe levels will generally decrease with increasing frequency, causing greater interference immunity.

Rear axis lobes will tend to remain constant as parabolic antennas are used at higher frequencies, resulting in no increased susceptibility to undesired emissions from this direction.

It can be concluded that the reference radiation pattern for large terrestrial parabolic antennas operating between 2 and 10 GHz* (Figure 8) is useful for caluclations of interference between services at millimeter wavelengths, since the far and back sidelobe levels of large millimeter antennas will generally be equal to or lower than those specified in the reference pattern. This reference pattern can be replaced with measured data when this data becomes available for millimeter wavelengths and should be regarded as provisional for these frequencies.

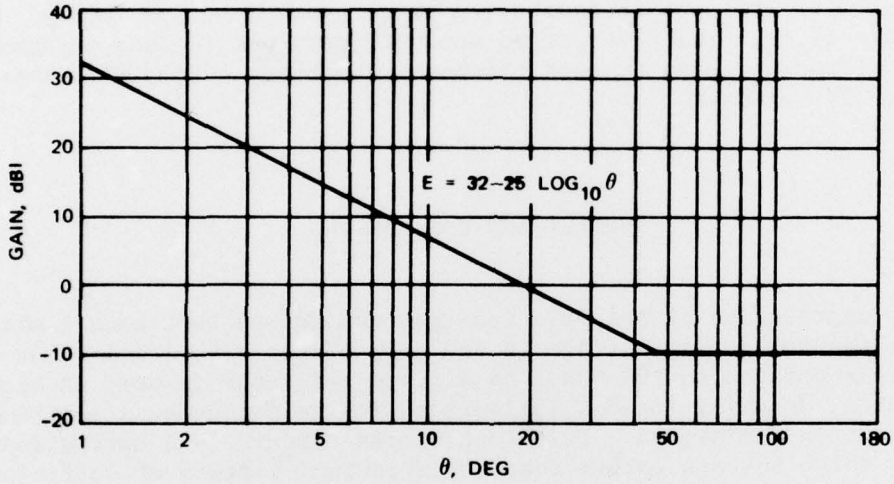

FIGURE 8. Provisional Reference Radiation Diagram (Levels Exceeded by 10% of Sidelobe Peaks; $D/\lambda > 100$).

*Presented in Report 391-2 and Recommendation 465-1 in Volume IV of the Green Books published at the Thirteenth Planning Assembly of the International Radio Consulation Committee (CCIR).